Thiol–Gelatin–Norbornene Bioink for Laser-Based High-Definition Bioprinting

Agnes Dobos, Jasper Van Hoorick, Wolfgang Steiger, Peter Gruber, Marica Markovic, Orestis G. Andriotis, Andreas Rohatschek, Peter Dubruel, Philipp J. Thurner, Sandra Van Vlierberghe, Stefan Baudis, and Aleksandr Ovsianikov*

Two-photon polymerization (2PP) is a lithography-based 3D printing method allowing the fabrication of 3D structures with sub-micrometer resolution. This work focuses on the characterization of gelatin–norbornene (Gel–NB) bioinks which enables the embedding of cells via 2PP. The high reactivity of the thiol-ene system allows 2PP processing of cell-containing materials at remarkably high scanning speeds (1000 mm s^{-1}) placing this technology in the domain of bioprinting. Atomic force microscopy results demonstrate that the indentation moduli of the produced hydrogel constructs can be adjusted in the 0.2–0.7 kPa range by controlling the 2PP processing parameters. Using this approach gradient 3D constructs are produced and the morphology of the embedded cells is observed in the course of 3 weeks. Furthermore, it is possible to tune the enzymatic degradation of the crosslinked bioink by varying the applied laser power. The 3D printed Gel–NB hydrogel constructs show exceptional biocompatibility, supported cell adhesion, and migration. Furthermore, cells maintain their proliferation capacity demonstrated by Ki-67 immunostaining. Moreover, the results demonstrate that direct embedding of cells provides uniform distribution and high cell loading independently of the pore size of the scaffold. The investigated photosensitive bioink enables high-definition bioprinting of well-defined constructs for long-term cell culture studies.

1. Introduction

The field of 3D bioprinting has demonstrated a considerable progress within the recent decade, with new or refined technologies and materials reported constantly.[1] However, until now, the low resolution of conventional technologies remained one of the main unconquered frontiers in 3D bioprinting.[2,3] Indeed, since most of 3D bioprinting methods rely on depositing the material with the cells, their resolution is few tens of micrometers at best and thus is not sufficient to recreate complex geometries, intrinsic architecture of the extracellular matrix (ECM), or to change the material properties on the subcellular level. Lithography-based approaches can overcome this limitation by locally crosslinking the material containing living cells instead of depositing it to create 3D geometries.[4] In particular, two-photon polymerization (2PP) is capable of spatial resolution well into sub-micrometer range. Due to the nonlinear nature of 2PP process, it is possible to produce structures directly within the volume of the sample.[5] The latter eliminates the need for a layer-by layer deposition or the addition of absorbers in order to limit penetration depth as in stereolithography and digital light processing.[6,7] It is often incorrectly anticipated that 2PP has a limited throughput due to the hardware limitations resulting in an extremely low scanning speed in the order of

A. Dobos, Dr. W. Steiger, Dr. P. Gruber, Dr. M. Markovic, Prof. A. Ovsianikov
TU Wien
3D Printing and Biofabrication Group
Institute of Materials Science and Technology
Getreidemarkt 9, 1060 Vienna, Austria
E-mail: Aleksandr.Ovsianikov@tuwien.ac.at

The ORCID identification number(s) for the author(s) of this article can be found under https://doi.org/10.1002/adhm.201900752.

A. Dobos, Dr. W. Steiger, Dr. P. Gruber, Dr. M. Markovic, Dr. O. G. Andriotis, A. Rohatschek, Prof. P. J. Thurner, Prof. A. Ovsianikov
Austrian Cluster for Tissue Regeneration

J. Van Hoorick, Prof. P. Dubruel, Prof. S. Van Vlierberghe
Polymer Chemistry and Biomaterials Group
Centre of Macromolecular Chemistry
Ghent University
Krijgslaan 281, S4, 9000 Ghent, Belgium

J. Van Hoorick, Prof. S. Van Vlierberghe
Brussels Photonics
Department of Applied Physics and Photonics
Flanders Make and Vrije Universiteit Brussel
Pleinlaan 2, 1000 Brussels, Belgium

Dr. O. G. Andriotis, A. Rohatschek, Prof. P. J. Thurner
TU Wien, Institute of Lightweight Design and Structural Biomechanics
Getreidemarkt 9, 1060 Vienna, Austria

Dr. S. Baudis
TU Wien
Institute of Applied Synthetic Chemistry
Getreidemarkt 9, 1060 Vienna, Austria

ADVANCED
SCIENCE NEWS
www.advancedsciencenews.com

ADVANCED
HEALTHCARE
MATERIALS
www.advhealthmat.de

tens to few hundred micrometers per second. However, already over 5 years ago our group has demonstrated that 2PP systems are capable of scanning as fast as 500–1000 mm s^{-1}.[8,9] When it comes to bioprinting, the main bottleneck for 2PP was availability of biocompatible and highly reactive material, supporting high-speed processing of cell-containing materials at moderate laser power.

Photosensitive polymers, including synthetic and natural, are often employed as bioinks for 3D bioprinting.[4,10] The main advantage of natural hydrogels is that they provide a close resemblance to the native environment of cells. They are often derived from the noncellular component of tissues, the extracellular matrix, which plays an important role in regulating cell proliferation, morphology and migration, both in embryonic development and pathological processes.[11]

Radical thiol-ene click reaction, based on the remarkably efficient reaction of thiols with non-homopolymerizable carbon–carbon double bonds, leads to a step-growth polymerization and network formation, via repeated addition of thiyl radials to double bonds and chain transfer reactions by hydrogen abstraction.[12] Thiol-ene reactions can be performed under mild conditions and can result in a highly biocompatible hydrogel. Since no homopolymerization occurs between the norbornene groups, it will only react with thiols in a stoichiometric ratio resulting in a single orthogonal covalent bond unlike (meth)-acrylate/amide-based hydrogels, which often form heterogeneous networks due to the formation of kinetic oligo(meth)acrylate chains.[12] Both natural and synthetic polymers have been functionalized with either thiol or "ene" moieties, including hyaluronic acid (HA), gelatin, and polyethylene glycol (PEG).[13–18]

Direct embedding of human mesenchymal stem cells (hMSCs) into gelatin–norbornene hydrogels (Gel–NB) was reported previously via UV-polymerization and resulted in higher cell survival when compared to standard methacrylamide gelatin (GelMA) based hydrogels.[15] In another report, matrix metalloproteinase degradable poly(ethylene glycol)-based thiol-ene hydrogels also proved useful for the encapsulation and differentiation of hMSCs into osteogenic, chondrogenic, and adipogenic lineage.[19] Thiol-ene click reactions can also be applied to alter the properties of the hydrogels after crosslinking without changing the base composition, as demonstrated by using unreacted norbornene functionalities on a partially crosslinked HA–norbornene gel to introduce secondary functionalities using thiol-ene photografting, thereby either locally changing the mechanical properties of the hydrogel or introducing localized functionalities after polymerization.[14]

Several different thiol/ene modified materials have been successfully employed with 2PP, including thiol-ene modified poly(vinyl alcohol), gelatin vinyl ester, and Gel–NB.[17,18,20] However, direct embedding of cells during 2PP processing while maintaining cell viability has only been achieved with GelMA bioinks.[21,22]

The present work focuses on the characterization of 3D printed Gel–NB based bioinks and the direct embedding of cells via 2PP. After optimization of polymer, crosslinker, and photoinitiator concentrations, the processing window for 2PP at 720 nm was established. 720 nm processing wavelength was chosen due to the better match to the absorption properties of the used diazosulfonate-based photoinitiator (DAS).[22] The mechanical properties of the hydrogel were characterized via atomic force microscopy (AFM) cantilever-based microindentation, and the equilibrium swelling and enzymatic degradation by collagenase was also determined. Direct embedding of L929 mouse fibroblast cells was performed via 2PP for long-term 3D cell culture studies, during which cell viability, proliferation, morphology, and migration were addressed. In addition, the cell loading capacity of direct embedding into porous scaffolds with a variety of pore sizes was compared to conventional scaffold seeding. Finally, the cells were embedded within 3D structures characterized by a crosslinking density gradient and the morphology of cells within different regions was observed in the course of 3 weeks. To our best knowledge, this is the first systematic study showing the possibility to produce cell-embedding hydrogel constructs by 2PP technology at a relatively high throughput, paving the way to high-definition (HD) bioprinting.

2. Results and Discussion

Based on our preliminary experiments (not shown), a concentration of 7.5 wt% Gel–NB supplemented with 0.5×10^{-3} M cleavable biocompatible diazosulfonate photoinitiator in phosphate buffered saline solution (PBS) was sufficient for producing stable structures at high writing speeds. The bifunctional low-molecular-weight dithiothreitol (DTT) was used as crosslinker.[17] The concentration of thiol groups using DTT was chosen to be equimolar in respect to the norbornene functionalities present on the gelatin, since in an ideal network an excessive amount of thiols results in a higher ratio of monoreacted thiol-groups while a lower amount results in unreacted norbornene functionalities, leading to incomplete network formation.[9]

To establish a processing window, different laser powers and writing speeds were tested on the hydrogel formulation. The schematic design of the 2PP setup used is depicted in **Figure 1**. An array of cubes was produced with writing speeds ranging from 100 to 1000 mm s^{-1} and the minimal power needed to obtain stable structures, also referred to as 2PP threshold, was established for each speed. With increasing speed, the structuring threshold increased from 15 to 40 mW (**Figure 2**a). Remarkably high speeds can be achieved with considerably lower laser powers when compared to similar material formulations using GelMA together with DAS or other chain-growth based gelatin derivatives.[22,23]

In an ideal case, if there are no irregularities in the hydrogel network due to unreacted functional groups and primary cycles (i.e., linking of different functionalities on the same gelatin chain to each other), the equilibrium swelling ratio should reach a constant value at a fixed monomer concentration.[24] Since the light dose has an effect on the crosslinking density, the equilibrium swelling of the samples as a function of writing speed and laser power was established. At the lower laser powers, which are close to the polymerization threshold, the swelling was higher due to a lower degree of crosslinking. In the upper average laser power range (60–100 mW), the equilibrium swelling of the cubes corresponded to the expected behavior of an ideal step-growth hydrogel network; hence, the swelling
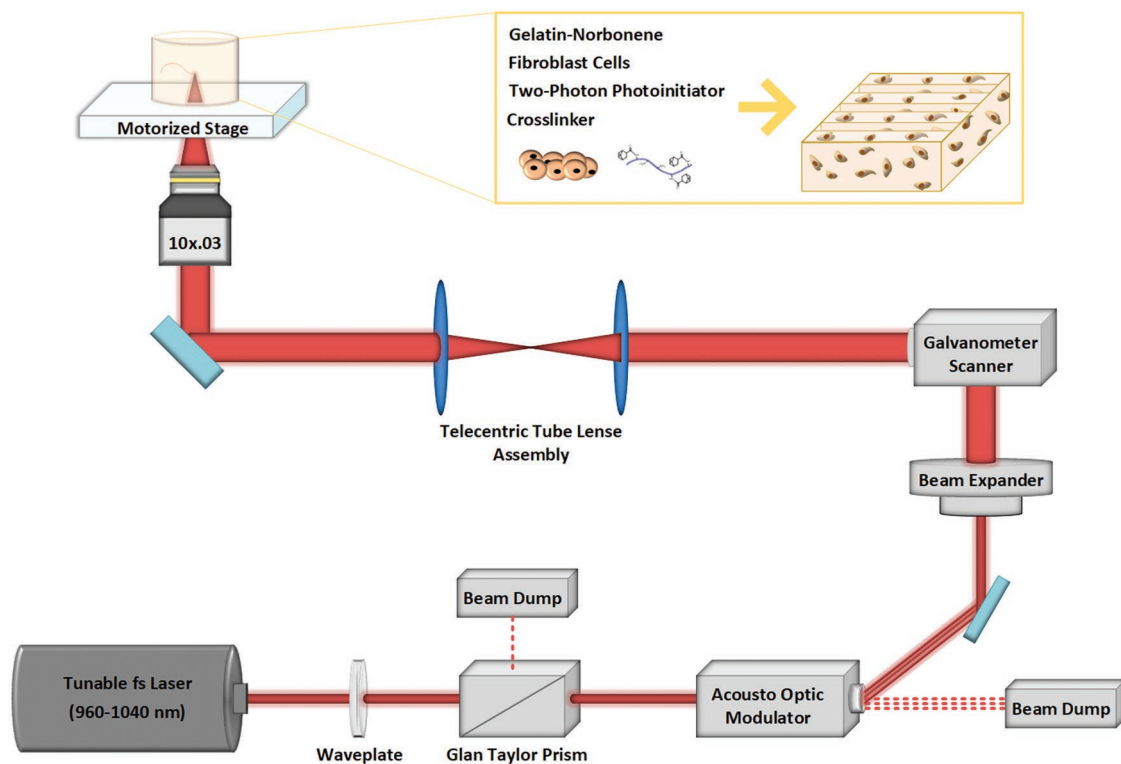
Figure 1. Schematic design of the used two-photon polymerization (2PP) setup.

ratio showed little variation between different writing speeds and powers (Figure 2b). Previous reports showed full conversion at a thiol-ene ratio of 1:1 with (Gel–NB)–DTT systems, whereas gels with a 0.5:1 ratio exhibited increased swelling and decreased stiffness.[17] However, our results at 100 mm s^{-1} (and to a lesser extent at 500 mm s^{-1}) indicate an increase in swelling toward higher laser powers. Furthermore, at 100 mm s^{-1} the swelling ratio was higher in every case compared to 500 and 1000 mm s^{-1}. We hypothesize that this behavior is the consequence of localized thermal effects, since at lower scanning speeds more energy is supplied per unit of time. It is known that the stability of DTT decreases drastically at increased temperatures.[25] Consequently, at 100 mm s^{-1} and at high laser intensities, the thiol/ene ratio will no longer remain equimolar due to degradation of the crosslinker. Second, due to the high irradiation energy, a large number of DTT molecules can be coupled to the norbornene functionality very fast, resulting in a drastic increase of viscosity. Hence, the diffusion of unreacted DTT molecules toward unreacted norbornene sites would be limited, resulting in weaker network formation.[18,26,27] Finally, at high exposure dose, the number of thiol radicals can be so high that termination occurs due to combination of two thiol radicals resulting in concurrent disulfide formation, thereby again resulting in non-equimolar thiol-ene ratios.[27,28]

Gelatin naturally contains amino acid sequences cleavable by matrix metalloproteinases (MMPs).[29] The degradation of the hydrogel caused by MMPs is mostly local events due to the short-range action of proteases. When exogenous collagenase is added at the concentration of 0.25 collagen digestion units (CDU) mL^{-1}, surface erosion is expected to be the main process. However, proteases can also diffuse into the hydrogel causing bulk degradation to some degree as well.[13,30,31] To assess this enzymatic degradability, hydrogel cubes printed at 1000 mm s^{-1} writing speed with three different laser powers were exposed to a collagenase enzyme and monitored using 3D laser scanning microscopy (LSM) every 5 min. An image analysis program developed in-house was used to determine the decrease of the volume of the structures over time (Figure S1, Supporting Information) independently of the mechanism of the degradation. By changing the laser power from 60 to 100 mW, the hydrogel degradation time increased substantially from 10 to 30 min, despite observing similar structure swelling behavior in this structuring range (Figure 2c).

Due to the small dimensions of the 2PP-produced hydrogel structures, characterization of their mechanical properties is not a trivial task. However, atomic force microscopy allows estimation of the indentation modulus (E) of relatively soft hydrogels on a microscale by employing cantilever-based microindentation.[32] The AFM results exhibited a close correlation between the stiffness of the 2PP-produced cubes and the hydrogel swelling. Structures produced at higher writing speeds (1000 mm s^{-1}) and lower laser powers (under 60 mW) were the softest (0.2–0.4 kPa). The maximum E indentation modulus was reached at 70 mW (0.7 kPa for 100 mm s^{-1}) before decreasing again at higher laser powers. With the faster writing speed of 1000 mm s^{-1}, E stayed constant at ≈0.5 kPa above 60 mW (Figure 2d), indicating complete crosslinking.

Directing cell alignment on a surface or in a 3D hydrogel construct has been reported in literature via several different approaches. Aligning cells in 2D has been performed via soft
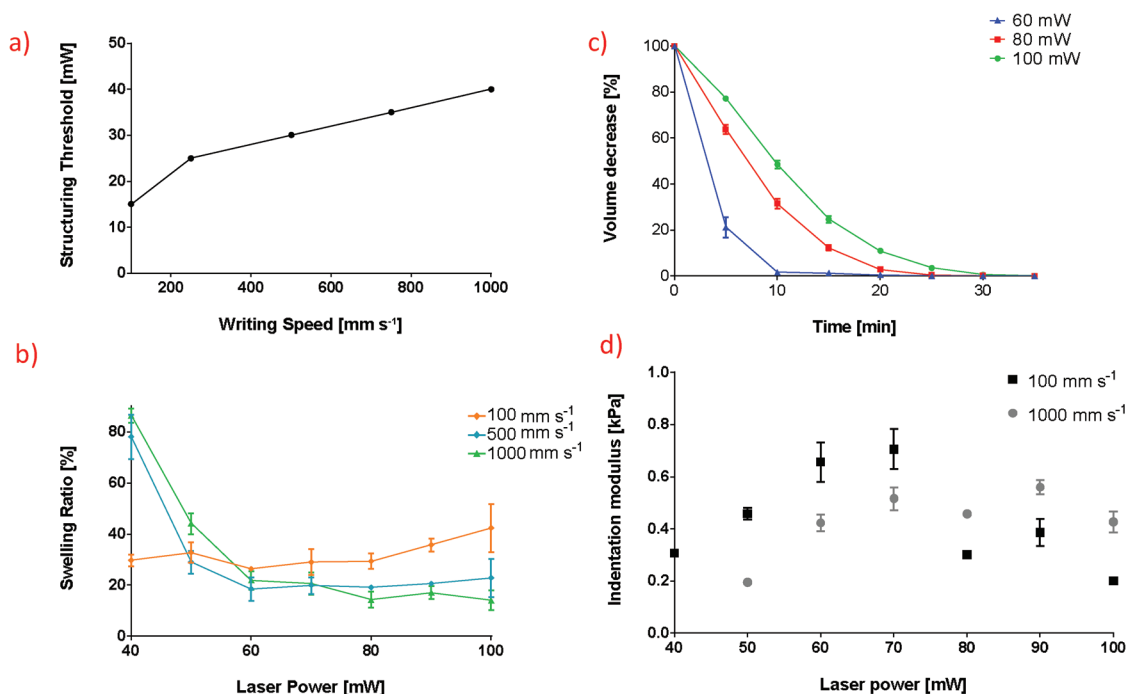
ADVANCED
SCIENCE NEWS
www.advancedsciencenews.com

ADVANCED
HEALTHCARE
MATERIALS
www.advhealthmat.de

Figure 2. Characterization of Gel–NB hydrogels. a) Structuring threshold of a 7.5 wt% Gel–NB hydrogel. Depending on the writing speed, different laser powers are needed to fabricate stable structures. By increasing the writing speed from 100 to 1000 mm s^{-1} the structuring threshold is increased by 25 mW. b) The swelling profile of the hydrogels shows low dependency on the writing speed or applied laser power indicating a fully crosslinked network. c) Different structuring powers (at 1000 mm s^{-1}) result in different degradation rates when exogenous collagenase (0.25 CDU mL^{-1}) was added. By increasing the laser power by 40 mW the acquired time for full degradation was three times higher. d) Atomic force microscopy measurements of Gel–NB hydrogels, processed at different writing speeds. Stiffness of the hydrogels was light dose dependent, with elastic moduli ranging between 0.2 and 0.7 kPa.

lithography or self-assembly to position pro-adhesive proteins on glass. However, most of the 2D methods involve micropatterning on rigid surfaces, which does not properly mimic in vivo conditions. Microengineered 3D matrices provide closer resemblance to the natural cell surrounding. Direct cell encapsulation via UV-polymerization and scaffold-based approaches have both been employed in order to control cell alignment and morphology.[33,34] One of the main disadvantages of such 3D cell culture systems is the lack of spatial control. Additive manufacturing approaches could provide a possible alternative to overcome this issue.

Due to the high resolution of 2PP, a high-throughput production of hydrogel-cell constructs by this technology requires high scanning speeds. Using 1000 mm s^{-1} writing speed, a 300 × 300 × 300 µm^3 cube could be printed in less than 10 min. Typically, high writing speeds require high photoinitiator concentrations or high laser powers which could damage the cells. However, by using the highly reactive thiol-ene photoclick chemistry it is possible to produce structures starting from 40 mW at a photoinitiator concentration of 0.5×10^{-3} M. This is a substantial improvement compared to conventional materials based on chain growth polymerization where 2×10^{-3} M of the same photoinitiator and approximately twice the light dose were needed to produce stable structures using higher monomer concentrations.[22,23] The reproducibility of the structures was maintained at the higher scanning speeds as the produced structures (Figure S2a, Supporting Information)

corresponded well with the computer-aided design (CAD) model (Figure S2b, Supporting Information). In order to validate the HD bioprinting parameters and their effect on cell survival, cubes were printed from the material containing L929 mouse fibroblast cells using a laser power range from 40 to 120 mW. The cells were co-stained with calcein AM/propidium iodide right after printing (postprinting) and after 24 h. The cell survival was close to 100% in the structures produced using laser powers below 100 mW and not significantly different for the two time points in the range of 40–100 mW (**Figure 3**a). However, above 100 mW a decrease of cell viability was observed and the cell survival dropped to 70% at 120 mW.

In order to demonstrate that the cells not only survive but also maintain their proliferative capacity, cubes with unidirectional channels were produced using laser powers ranging from 50 to 90 mW. In this respect, the cells, which are encapsulated in the structure (channels) but not directly exposed to laser radiation, can be compared to the cells embedded in the crosslinked material using different laser powers (Figure 3a). After 1 week in culture, the cells were fixed and anti-Ki-67 antibody with a secondary antibody labeled with Alexa-488 was applied to image proliferating cells using LSM. Additionally, the cell nucleus was stained using 4′,6-diamidino-2-phenylindole (DAPI) nuclear stain. Ki-67 is a frequently used marker which is present during all active phases of the cell cycle but absent in quiescent cells.[35] The results demonstrated that 77% of the cells encapsulated in the structure channels were positive
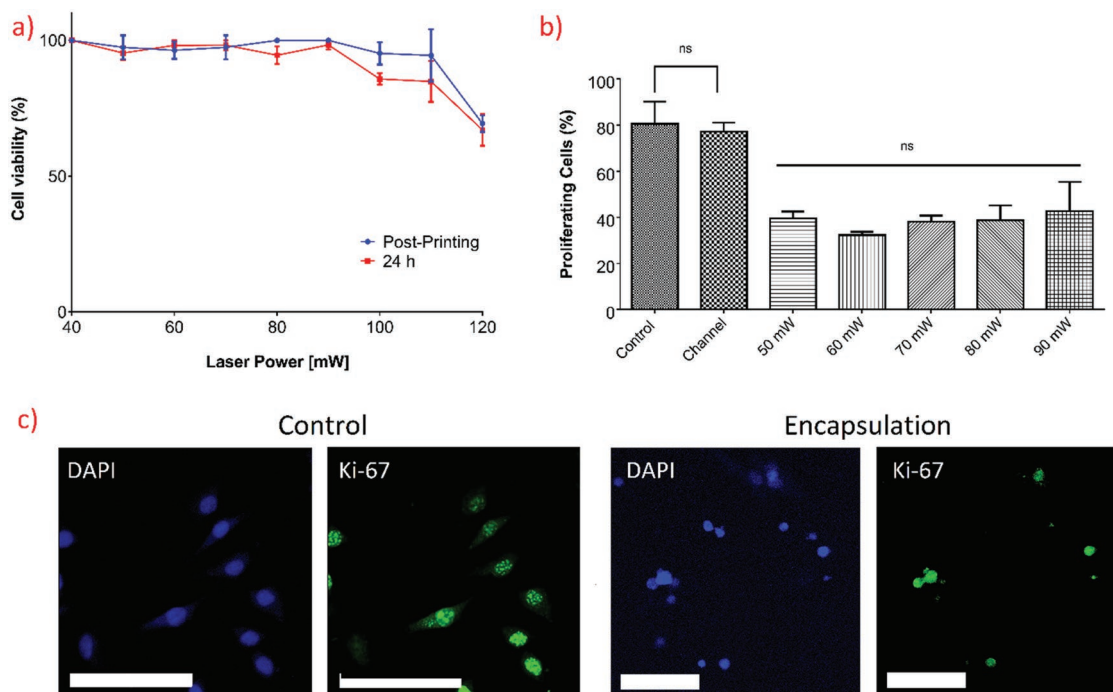
Figure 3. Direct encapsulation of L929 mouse fibroblasts in 7.5% Gel–NB hydrogels. a) 1 million mL^{-1} L929 cells were embedded using different laser powers (40–120 mW) at 1000 mm s^{-1}. The cells were stained with calcein AM/propidium iodide to address cell viability. Cell survival was only impaired above 110 mW. b) Proliferation of cells after 1 week of encapsulation. Cells embedded in cubes printed with different laser powers and stained with anti-Ki-67 antibodies, visualized using an Alexa-488 labeled secondary antibody. The cells were costained with a DAPI nuclear stain. The cells in the nonirradiated regions (channels) were not significantly different from the 2D control. A drop in the proliferation to ≈35% can be seen after encapsulation. The studied laser power does not affect the proliferation rate in the studied regions. c) Ki-67 staining of cells. The control cells (2D) show a more extended morphology after 1 week with the vast majority of the cells stained positive to Ki-67. The embedded cells show a more round morphology with ≈35% of cells being in the active phase. The scale bar represents 100 µm. The statistical significance was addressed by one way analysis of variance (ANOVA) followed by Bonferroni post-test.

to the Ki-67 marker, which was not significantly different from the 2D control cells (83%). However, the cells embedded in the crosslinked region between 50 and 90 mW had a decreased proliferation, between 32% and 40% of the cells being in the active phases of the cell cycle (Figure 3b). The laser power within this studied range did not result in any significant differences in observed cell proliferation. Although the number of proliferating cells embedded in the crosslinked hydrogel is approximately half of the control, the cells maintain the capacity to proliferate in 2PP-produced constructs (Figure 3c).

Another important factor apart from cell viability and proliferation is the ability of the cells to migrate within their surrounding matrix. The morphology and migration of cells is highly dependent on the mechanical properties of their environment.[36] By changing the laser power, it was possible to tune the indentation modulus of the hydrogel between 0.2 and 0.6 kPa. In order to demonstrate the effect of stiffness on cell morphology and migration, cells were embedded in a cube produced using an inverse Gaussian power distribution with the highest power being 85 mW and the lowest 45 mW at the center of the cube corresponding to a stiffness of 0.6 and 0.2 kPa, respectively (**Figure 4**a). The polymerized material exhibits some autofluorescence and its intensity corresponds to the applied laser power and concomitant network density (Figure 4b). The embedded mCherry labeled L929 cells exhibit a round morphology after one day of encapsulation. However,

after 3 weeks of culture, the cells in the softest region (i.e., in the middle) are extended and start to migrate toward the stiffer outer regions, while the cells in the stiffer regions stay round even after 3 weeks (Figure 4c).

To further demonstrate the potency of the reported system, mCherry labeled L929 cells were embedded in scaffolds with different pore sizes (10–40 µm). As a control, the scaffolds of identical design were printed and subsequently seeded with the same number of cells (1 million per mL). After printing, the cells were manually counted. The pore size did not affect initial cell numbers in direct encapsulation, and after 7 days the cell numbers increased in all cases. As we demonstrated earlier, cells encapsulated in the channels proliferate faster compared to cells embedded in crosslinked material. Therefore, the increase in cell numbers was more pronounced in the larger pore sized scaffolds (40 µm pore size, from 37 to 78 cells in average) in comparison to the small pore sized structures (10 µm, from 37 to 50 cells in average) due to the larger volume of the channels relative to the crosslinked material volume (**Figure 5**b). However, the cell seeding efficiency in the control group was highly dependent on the pore size: 10 µm pore sized scaffolds had no cells inside the structures, whereas the 40 µm ones had ≈18 cells per structure, corresponding to only half of the cells in the direct encapsulation experiments (Figure 5a).

Finally, to study long term survival of cells, mCherry L929 cells were encapsulated in a Gel–NB hydrogel construct with
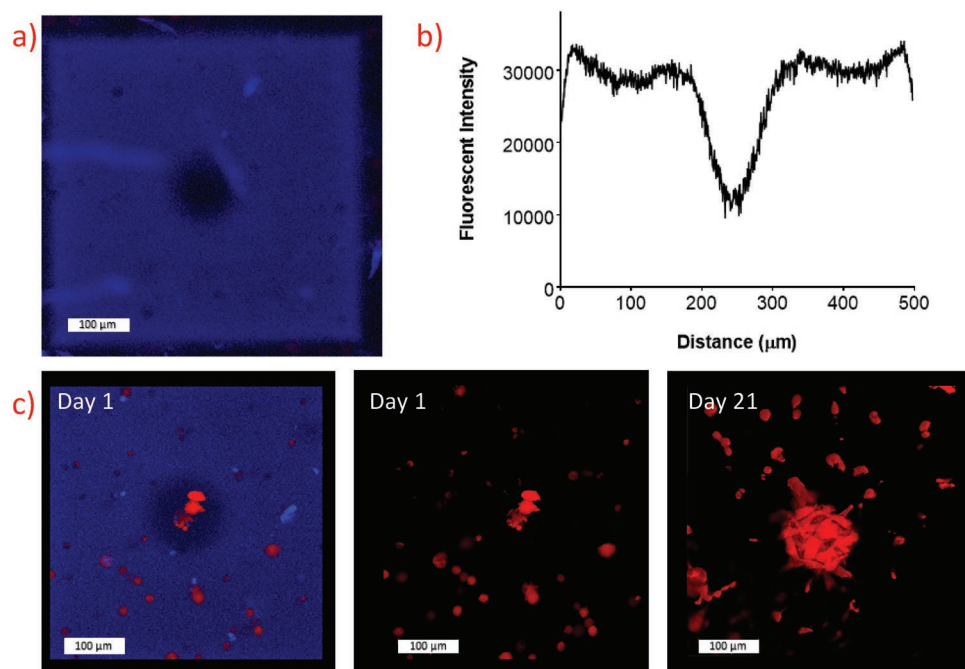
**ADVANCED
SCIENCE NEWS**

www.advancedsciencenews.com

**ADVANCED
HEALTHCARE
MATERIALS**

www.advhealthmat.de

Figure 4. Morphology and migration of embedded cells in a stiffness gradient cube. a) Cube printed with a centrosymmetric inverse Gaussian power distribution between 45 and 85 mW. b) The autofluorescence of the material was analyzed using ImageJ and it corresponds to the expected power distribution. c) mCherry labeled L929 cells embedded in the power gradient cube. After day 1, all cells in the matrix show round morphology while after day 21, cells in the middle softer region are more extended and are migrating toward the stiffer areas as well.

an interconnected channel network (with a 20 µm pore size) and wall structure around the perimeter to seal off the channels. After the first week of culture, the cells in the construct remained round along the channels of the printed construct. By week 3, cells aligned along the channels and filled the available space provided by the interconnected network. By week 5, the cells also started to migrate in the crosslinked regions, possibly by partially degrading the crosslinked material (**Figure 6**). To the best of our knowledge, this is the first manuscript reporting that structure degradation and controlled cell alignment is observed in structures produced via 2PP. Furthermore, the cells can be cultured at least up to 5 weeks in bioprinted Gel–NB hydrogel constructs, which makes long-term studies possible.

3. Conclusion

The use of Gel–NB hydrogels with an appropriate photoinitiator enabled high-definition bioprinting. Due to the quasi-ideal behavior and associated fast crosslinking kinetics of this material, a wide range of processing parameters (laser power and writing speed) is supported without a strong variation the mechanical properties of the produced hydrogels. Nevertheless, the degradation of the produced hydrogel constructs can be fine-tuned by varying the applied laser power. Close to the structuring threshold, the properties of the crosslinked material can be controlled by only slight variations of exposure dose. This allows the realisation of 3D structures with controlled swelling behavior and gradients of mechanical properties. Our

results demonstrate that within the used laser power range of up to 100 mW, viability and proliferation of the cells embedded in the hydrogel did not vary. Compared to scaffold seeding, a more uniform cell loading and higher cell densities can be achieved via high-definition bioprinting regardless of the pore size. Decoupling the possibility to produce small pores and constructs with complex high-resolution features from the cell-loading efficiency allows designing and executing systematic experiments on cell–material and cell–cell interactions in 3D for both developmental studies and disease progression models.

4. Experimental Section

Unless stated otherwise, all chemicals and cell culture reagents were purchased from Sigma-Aldrich (St. Louis, MO, USA). All graphs were plotted using GraphPad Prism 6.

Gel–NB Hydrogel Preparation: Gel–NB with a degree of substitution of 53% was synthesized following a previously reported protocol.[17] For the laser processing experiments, Gel–NB was dissolved in phosphate buffered saline solution to obtain a final concentration of 7.5 wt% at 37 °C. After complete dissolution, 0.5×10^{-3} M of the photoinitiator DAS and the crosslinker (DTT) at an equimolar thiol-ene ratio were added. Next, 30 µL of the obtained solution was pipetted into a silicone mold with a diameter of 6 mm and height of 1 mm placed on the methacrylated glass bottom dishes.[22]

Cell Culture: L929 mouse fibroblast cells and L929 cells labeled with mCherry (provided by Ludwig-Boltzmann Institute, Vienna, Austria) were cultivated at 37 °C and 5% CO_2 in the incubator. The retroviral transfection of the cell line is described elsewhere.[37] Cells were cultured in DMEM high glucose media supplemented with 1% penicillin–streptomycin solution and 10% fetal calf serum. Upon 90% confluency, the cells were detached using 0.5% trypsin-EDTA solution
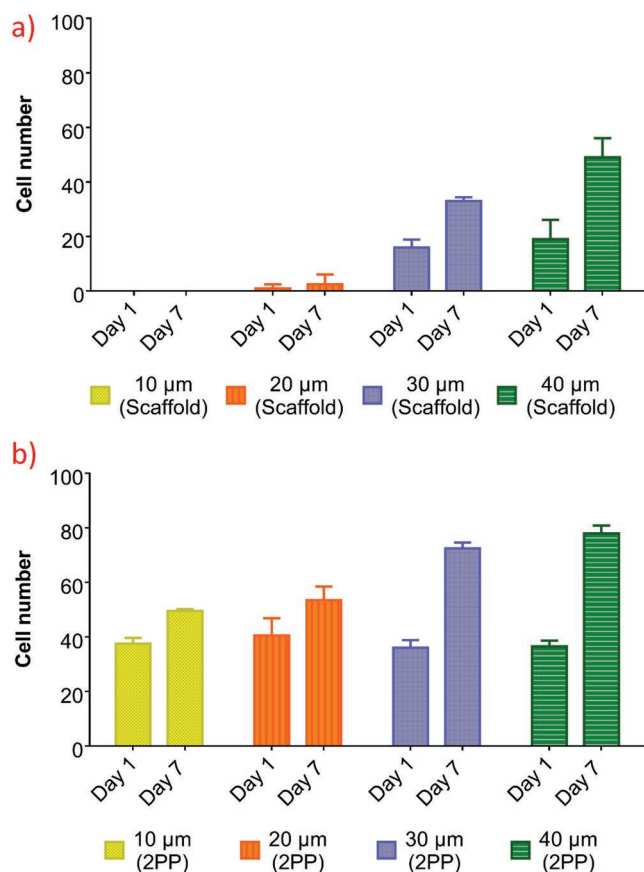
Figure 5. Cell loading capacity of direct cell encapsulation compared to scaffold seeding. a) Cell numbers after seeding and 7 days. The smallest pore sized scaffold (10 μm) could not retain any cells during drop-seeding, while with increasing pore sizes the cell numbers increased as well (20 μm: 1 cell, 30 μm: 16 cells, 40 μm: 18 cells in average). b) Cell numbers after seeding and 7 days in direct embedded samples. The initial cell numbers were not significantly different between different pore size samples (10 μm: 37 cells, 20 μm: 40 cells, 30 μm: 36 cells, 40 μm: 37 cells on average).

and centrifuged at 170 g for 5 min followed by plating in T75 flasks (VWR, Radnor, USA)

Laser Setup: A tunable femtosecond laser with a repetition rate of 80 MHz (MaiTai eHP DeepSee, Spectra-Physics) was operated at 720 nm, with a pulse duration of 70 fs after the microscope objective (Plan-Apochromat, 10x/0.3, Zeiss, Oberkochen, Germany). In order to ensure high-resolution printing, the sample and laser positioning were performed using a motorized microscope stage and dual-axis galvanometric scanner, respectively. For data processing, the corresponding 3D CAD file was sliced into layers of 0.5 μm and a hatch spacing of 0.5 μm. A schematic of the printer is described in Figure 1. The acousto optic modulator is used for fast switching of the laser and telecentric lense assembly ensures that be beam stays on the back aperture of the objective.

Methacrylation of Glass Slides: To ensure proper attachment of the 3D printed hydrogel structures to the substrate, the glass surfaces were modified with methacrylate functionalities following a silanization procedure using 3-(trimethoxysilyl)propyl methacrylate prior to the structuring. All structures were printed in glass bottom dishes (IBIDI 35 mm diameter with glass bottom, high version, Ibidi GmbH, Martinsried, Germany). The glass surfaces were plasma treated (Harrick plasma, Ithaca, USA) for 10 min prior to the addition of the methacrylation solution (50% deionized water, 48% ethanol, 0.3% acetic acid, and 2% of

3-(trimethoxysilyl)propyl-methacrylate) for 45 min. Afterward, the glass dishes were washed with deionized water and dried at room temperature. The dishes were sterilized by UV irradiation before cell culture use.

Structuring Threshold: 100 μm × 100 μm cubes were printed in the above-mentioned hydrogel formulation with different laser powers (10–100 mW) and scanning speeds ranging from 100 to 1000 mm s^{-1}. Afterward, the unpolymerized material was washed away with PBS at 37 °C and the cubes were imaged using bright-field optical microscopy (Zeiss, Oberkochen, Germany). The threshold was defined as the minimal required laser power to yield a stable structure.

Equilibrium Swelling: The above-mentioned 100 μm × 100 μm cubes were printed followed by incubation at 37 °C in PBS overnight. The swelling ratio of the hydrogels was obtained semiquantitatively, by measuring the surface area of the top of the CAD image and comparing this to the surface area of the top slice of the printed cube. The swelling was calculated by the following formula (Equation (1))

$$Q = \frac{A_{cube} - A_{CAD}}{A_{CAD}} \times 100 \tag{1}$$

where Q is the swelling ratio, and A is the surface area in μm^2.

Degradation Scanner: The degradation of the hydrogel was performed using collagenase from *Clostridium histolyticum*. To this end, 100 μm × 100 μm hydrogel cubes were structured at 1000 mm s^{-1} using 60, 80, or 100 mW and incubated in PBS overnight at 37 °C to reach equilibrium swelling. Afterward, a 1 mg mL^{-1} 2000 kDa FITC labeled dextran (TdB Consultancy AB, Uppsala, Sweden) was added to the collagenase solution to make fluorescent imaging possible. The collagenase solution was added to the samples at a final concentration of 0.25 CDU mL^{-1} and time lapse Z-stacks of the cubes were recorded every 5 min using confocal laser scanning microscopy (Zeiss, Oberkochen, Germany).

The degradation scanner is an analytical tool that was developed to quantify the change in volume of a 3D structure. Using Z-stack images obtained from the LSM microscope, a python-based code reads the images for each layer. The image is separated into a grid which can be adjusted by the viewer. Translating the image data into an array of 8-bit values allows determination of threshold intensity. This intensity value is used to discriminate between solid structures (dark areas in Figure S1, Supporting Information) and surrounding liquid. For each region, the pixels which meet the criterion are summed up and multiplied using the image conversion factor (obtained with the image analysis tool from a reference structure). Knowing the surface (μm^2) of a single pixel as well as the distance between each layer image allows the calculation of the volume of each structure. Adding the results for each area and each layer enables to do the calculation of the total volume of each structure and different time points until the structures are fully degraded.

Atomic Force Microscopy: Atomic force microscopy experiments were performed on a NanoWizard ULTRA Speed AFM system (JPK Instruments AG, Berlin, Germany) equipped with an inverted optical microscope (Axio Observer.D1, ZEISS). Unless otherwise specified, AFM cantilever-based microindentation experiments were performed with the MSNL (0.01 N m^{-1} nominal spring constant, cantilever C) (Bruker, Billerica, MA, USA). Prior to mechanical assessment, the thermal noise method was used to determine the spring constant of the cantilever.[38] The measured spring constant of the cantilever was 0.0062 N m^{-1}. Then, the cantilever was furnished with a colloidal probe made of borosilicate glass.[32,39] The radius of the colloidal probe was determined via atomic force microscopy imaging of a calibration grating (TGT1, NDTMT).[32] AFM cantilever-based indentation experiments were performed in PBS (pH 7.5) on hydrated samples and in force control with a maximum applied load of 1 nN at room temperature. One to two force volume maps were recorded per sample with a 4 × 4 pixel resolution resulting in 16 to 32 force-indentation curves per sample. The indentation modulus was estimated by analyzing the unloading part of the force–indentation curves as described previously using the Oliver–Pharr method.[32,40] All force–indentation data were processed in a custom built Matlab script (2015b, The MathWorks Inc., Natick, Massachusetts, United States.)
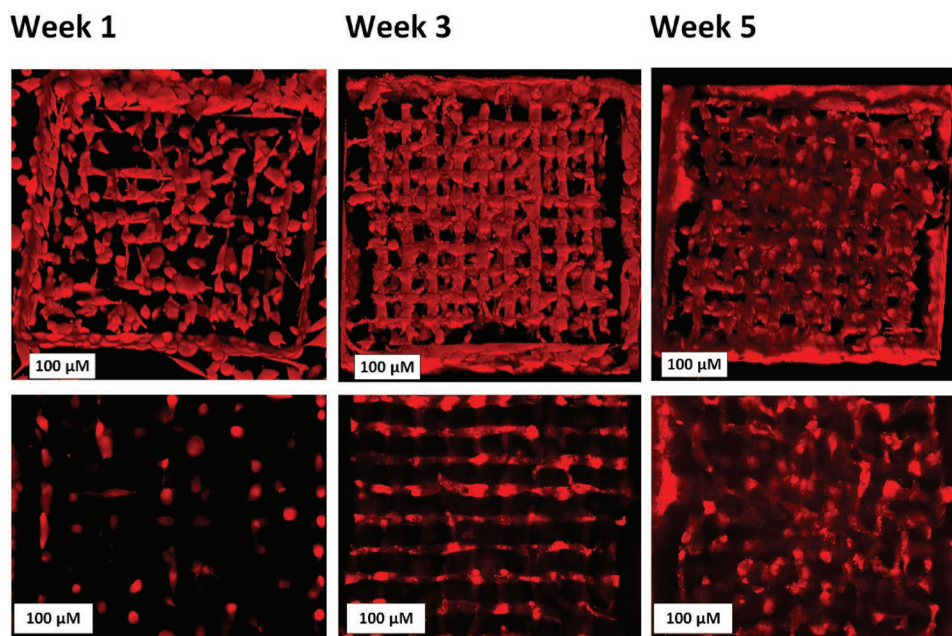
Figure 6. mCherry labeled L929 fibroblast cells embedded in 7.5 wt% GelNB hydrogels. The top row shows the 3D Z-stack of the fabricated hydrogels, while the bottom row displays a single layer of the structures. After 1 week, the cells exhibited a rounded morphology throughout the structure. By week 3, the cells aligned along the fabricated channels and filled up the available space. Finally, after 5 weeks, the cells partially degraded the hydrogel and migrated into the crosslinked sections of the hydrogel as well.

Cell-Containing Hydrogels: The cells were trypsinized and resuspended at 1×10^6 cells mL^{-1} in 7.5% Gel–NB supplemented with 0.5×10^{-3} M DAS and DTT at an equimolar thiol-ene ratio. The hydrogel precursor solution was pipetted into the aforementioned silicone mold in glass bottom methacrylated dishes.

Cell Viability: In order to assess the cell viability after printing, L929 cells were embedded using the above-mentioned protocol in $200 \times 200 \times 200$ μm^3 cubes printed at 1000 mm s^{-1} writing speed and different laser powers (40–120 mW). After printing, the structures were immersed in cell culture medium at 37 °C for 1 h to remove the nonpolymerized material. Afterward, the cells were stained with calcein AM/propidium iodide live–dead staining according to the manufacturer's protocol for 30 min before LSM images were taken. After imaging, the cell culture media were changed and the staining was repeated 24 h later. The number of dead and alive cells was counted manually.

Ki-67 Immunostaining: In order to address the effect of the different stiffnesses on proliferation, mCherry L929 cells were embedded in the above-mentioned fashion in a cube with unidirectional channels printed with different laser powers. The cells were incubated in cell culture medium for 1 week before fixation using 4% Histofix (Carl Roth GmbH, Karlsruhe, Germany) for 1 h. Afterward, the fixed structures were washed with PBS and permeabilized with 0.5% Triton-X in 1 wt% bovine serum albumin dissolved in PBS (PBS-BSA) for 15 min. The nonspecific absorption of the antibodies was blocked by incubation with PBS-BSA for 15 min prior to the addition of primary anti-Ki-67 antibodies (Abcam, Cambridge, United Kingdom) in a dilution of 1:200 overnight at 4 °C. Afterward, the cells were washed three times for 5 min with PBS-BSA before the addition of the Goat anti-Rabbit IgG (H+L) Superclonal Secondary Antibody, Alexa Fluor 488 (Thermo-Fisher, Waltham, MA, USA) for 2 h. Next, the structures were washed again two times for 5 min with PBS-BSA before the addition of DAPI (Biotium Inc., Fremont, CA, USA) in a dilution of 1:200 in PBS-BSA for 1 h. The cells were imaged using LSM and the number of proliferating cells and cell nuclei were counted both in the crosslinked hydrogel and in the channels. As control, cells growing on glass substrate were used.

All structures were printed with a laser writing speed of 1000 mm s^{-1}.

Power Distribution: To assess the effect of material stiffness in the achievable range, a $500 \times 500 \times 200$ μm^3 cube with an inverse Gaussian power distribution with laser powers ranging from 85 down to 45 mW was produced. The autofluorescence of the material was imaged using LSM. The fluorescence intensity of the cross-section of the cube was analyzed using ImageJ. Afterward, mCherry L929 cells were embedded in 7.5% Gel–NB hydrogels using the above-mentioned protocol and the inverse Gaussian cube was structured. The cell morphology was assessed by imaging the cells in the different regions of the cube over 3 weeks.

Scaffold Seeding and Direct Cell Encapsulation: Gel–NB scaffolds with different pore sizes (10–40 μm) were produced using 7.5% Gel–NB supplemented with 0.5×10^{-3} M DAS and an equimolar thiol/ene ratio of DTT. The constructs were developed in cell culture media and incubated overnight before the seeding of mCherry L929 cells at a concentration of 1×10^6 cells mL^{-1}. The cells were left to sediment and attach for the same time as the direct encapsulation takes (≈1 h). The same porous structures and concentration of cells were used for direct encapsulation using the above-mentioned protocol. After printing, the constructs were immersed in cell culture media. All structures, both for direct encapsulation and seeded scaffolds, were printed using 90 mW laser power and 1000 mm s^{-1} writing speed. Images were taken using LSM 700. The cells in the structure were counted manually. All cells which attached to the top and to the sides of the structures were disregarded.

Supporting Information

Supporting Information is available from the Wiley Online Library or from the author.

Conflict of Interest

The authors declare no conflict of interest.

Keywords

[1] A. Ovsianikov, J. Yoo, V. Mironov, *3D Printing and Biofabrication*, Springer, Berlin **2018**.

[2] S. V Murphy, A. Atala, *Nat. Biotechnol.* **2014**, *32*, 773.

[3] A. K. Miri, I. Mirzaee, S. Hassan, S. Mesbah Oskui, D. Nieto, A. Khademhosseini, Y. S. Zhang, *Lab Chip* **2019**, *19*, 2019.

[4] K. Hölzl, S. Lin, L. Tytgat, S. Van Vlierberghe, L. Gu, A. Ovsianikov, *Biofabrication* **2016**, *8*, 032002.

[5] A. Ovsianikov, V. Mironov, J. Stampfl, R. Liska, *Expert Rev. Med. Devices* **2012**, *9*, 613.

[6] K. S. Lim, R. Levato, P. F. Costa, M. D. Castilho, C. R. Alcala-Orozco, K. M. A. van Dorenmalen, F. P. W. Melchels, D. Gawlitta, G. J. Hooper, J. Malda, T. B. F. Woodfield, *Biofabrication* **2018**, *10*, 034101.

[7] B. Grigoryan, S. J. Paulsen, D. C. Corbett, D. W. Sazer, C. L. Fortin, A. J. Zaita, P. T. Greenfield, N. J. Calafat, J. P. Gounley, A. H. Ta, F. Johansson, A. Randles, J. E. Rosenkrantz, J. D. Louis-Rosenberg, P. A. Galie, K. R. Stevens, J. S. Miller, *Science* **2019**, *364*, 458.

[8] P. E. Petrochenko, J. Torgersen, P. Gruber, L. A. Hicks, J. Zheng, G. Kumar, R. J. Narayan, P. L. Goering, R. Liska, J. Stampfl, A. Ovsianikov, *Adv. Healthcare Mater.* **2015**, *4*, 739.

[9] A. Ovsianikov, Z. Li, J. Torgersen, J. Stampfl, R. Liska, *Adv. Funct. Mater.* **2012**, *22*, 3429.

[10] P. S. Gungor-Ozkerim, I. Inci, Y. S. Zhang, A. Khademhosseini, M. R. Dokmeci, *Biomater. Sci.* **2018**, *6*, 915.

[11] C. Frantz, K. M. Stewart, V. M. Weaver, *J. Cell Sci.* **2010**, *123*, 4195.

[12] C. E. Hoyle, C. N. Bowman, *Angew. Chem., Int. Ed.* **2010**, *49*, 1540.

[13] C. C. Lin, C. S. Ki, H. Shih, *J. Appl. Polym. Sci.* **2015**, *132*, 41563.

[14] W. M. Gramlich, I. L. Kim, J. A. Burdick, *Biomaterials* **2013**, *34*, 9803.

[15] Z. Münoz, H. Shih, C.-C. Lin, *Biomater. Sci.* **2014**, *2*, 1063.

[16] S. Van Vlierberghe, E. Schacht, P. Dubruel, *Eur. Polym. J.* **2011**, *47*, 1039.

[17] J. Van Hoorick, P. Gruber, M. Markovic, M. Rollot, G. Graulus, M. Vagenende, M. Tromayer, J. Van Erps, H. Thienpont, J. C. Martins, S. Baudis, A. Ovsianikov, P. Dubruel, S. Van Vlierberghe, *Macromol. Rapid Commun.* **2018**, *39*, 1800181.

[18] S. Baudis, D. Bomze, M. Markovic, P. Gruber, A. Ovsianikov, R. Liska, *J. Polym. Sci., Part A: Polym. Chem.* **2016**, *54*, 2060.

[19] S. B. Anderson, C.-C. Lin, D. V. Kuntzler, K. S. Anseth, *Biomaterials* **2011**, *32*, 3564.

[20] X.-H. Qin, J. Torgersen, R. Saf, S. Mühleder, N. Pucher, S. C. Ligon, W. Holnthoner, H. Redl, A. Ovsianikov, J. Stampfl, R. Liska, *J. Polym. Sci., Part A: Polym. Chem.* **2013**, *51*, 4799.

[21] M. Tromayer, P. Gruber, M. Markovic, A. Rosspeintner, E. Vauthey, H. Redl, A. Ovsianikov, R. Liska, *Polym. Chem.* **2017**, *8*, 451.

[22] M. Tromayer, A. Dobos, P. Gruber, A. Ajami, R. Dedic, A. Ovsianikov, R. Liska, *Polym. Chem.* **2018**, *9*, 3108.

[23] J. Van Hoorick, P. Gruber, M. Markovic, M. Tromayer, J. Van Erps, H. Thienpont, R. Liska, A. Ovsianikov, P. Dubruel, S. Van Vlierberghe, *Biomacromolecules* **2017**, *18*, 3260.

[24] H. Shih, C.-C. Lin, *Biomacromolecules* **2012**, *13*, 2003.

[25] R. Stevens, L. Stevens, N. C. Price, *Biochem. Educ.* **1983**, *11*, 70.

[26] B. D. Fairbanks, S. P. Singh, C. N. Bowman, K. S. Anseth, *Macromolecules* **2011**, *44*, 2444.

[27] R. F. Pereira, P. J. Bártolo, *Engineering* **2015**, *1*, 90.

[28] T. O. Machado, C. Sayer, P. H. H. Araujo, *Eur. Polym. J.* **2017**, *86*, 200.

[29] T. Greene, T. Lin, O. M. Andrisani, C. Lin, *J. Appl. Polym. Sci.* **2017**, *134*, 44585.

[30] A. A. Aimetti, A. J. Machen, K. S. Anseth, *Biomaterials* **2009**, *30*, 6048.

[31] A. Ovsianikov, A. Deiwick, S. Van Vlierberghe, P. Dubruel, L. Möller, G. Drager, B. Chichkov, *Biomacromolecules* **2011**, *12*, 851.

[32] L. Kain, O. G. Andriotis, P. Gruber, M. Frank, M. Markovic, D. Grech, V. Nedelkovski, M. Stolz, A. Ovsianikov, P. J. Thurner, *J. Mech. Behav. Biomed. Mater.* **2018**, *85*, 225.

[33] Y. Li, K. A. Kilian, *Adv. Healthcare Mater.* **2015**, *4*, 2780.

[34] M. A. Skylar-Scott, M.-C. Liu, Y. Wu, A. Dixit, M. F. Yanik, *Adv. Healthcare Mater.* **2016**, *5*, 1233.

[35] T. Scholzen, J. Gerdes, *J. Cell. Physiol.* **2000**, *182*, 311.

[36] M. Ehrbar, A. Sala, P. Lienemann, A. Ranga, K. Mosiewicz, A. Bittermann, S. C. Rizzi, F. E. Weber, M. P. Lutolf, *Biophys. J.* **2011**, *100*, 284.

[37] L. Knezevic, M. Schaupper, S. Mühleder, K. Schimek, T. Hasenberg, U. Marx, E. Priglinger, H. Redl, W. Holnthoner, *Front. Bioeng. Biotechnol.* **2017**, *5*, 25.

[38] J. L. Hutter, J. Bechhoefer, *Rev. Sci. Instrum.* **1993**, *64*, 1868.

[39] C. Neto, V. S. Craig, *Langmuir* **2001**, *17*, 2097.

[40] W. C. Oliver, G. M. Pharr, *J. Mater. Res.* **1992**, *7*, 1564.